Advances in Molecular Relaxation and Interaction Processes, 24 (1982) 123—138
Elsevier Scientific Publishing Company, Amsterdam — Printed in The Netherlands

MOLECULAR DYNAMICS SIMULATION OF LIQUID CHLOROFORM

MYRON W. EVANS

Chemistry Department, University College of Wales, Aberystwyth, Dyfed SY23 1NE

(Received 14 April 1982)

ABSTRACT

A molecular dynamics simulation of $CHCl_3$ is reported using a 5 x 5 Lennard-Jones atom-atom potential with partial charges at each atomic site. Thermodynamic and spectral properties have been computed for direct comparison with a range of experimental measurements. In general the agreement is good, given the semi-empirical nature of the pair potential used. Having checked the efficiency of the simulation in this way it is possible to use the algorithm to investigate molecular properties of liquid $CHCl_3$ which are not easily detectible with experimental or purely (non-numerical) theoretical methods. A range of mixed autocorrelation functions of the type $\langle A(o)B(t)\rangle$ has been used in this way to investigate: a) non Gaussian effects in the liquid state of $CHCl_3$; b) non-linear effects; c) rotation/translation effects too subtle for detection with present-day spectroscopic methods. It is clear that the classical theory of the Brownian motion [12] is in need of development because the simulation shows that it is not possible to factorise conditional probability density functions of rotation and translation into purely constituent parts. The pair-potential could be improved if measurements on the second dielectric virial coefficient of $CHCl_3$ vapour were to become available over a sufficient range of density.

INTRODUCTION

The use of molecular dynamics simulation to investigate the liquid state of matter is dependent on the availability of quantitative intermolecular pair potentials [1]. Until such potentials are measured through the dielectric virial coefficient [2] B_ε for example we are forced to rely on semi-empirical models. The use of these models finds justification in transferable parameters, i.e. if the atom-atom Lennard-Jones factors ϵ/k and σ used for $CHCl_3$ can also be used for

0378-4487/82/0000—0000/$02.75

the other chloromethanes [3] we are beginning to develop a predictive numerical method of describing the complete range of liquid state properties available to us. If such a method can be shown to work with experimental variables such as spectral bandshapes [4,5] whose origins can be traced analytically to well-known autocorrelation functions (a.c.f.'s) of molecular properties then it can also be used in the predictive sense to investigate subtler molecular dynamical properties that present-day spectroscopy cannot easily discern.

This overall methodology is used in paper to investigate the molecular dynamics of liquid chloroform ($CHCl_3$) at 293K, 1 bar. A molecular dynamics algorithm is developed to compute the thermodynamic and spectral properties of interest from the equations of motion of 108 $CHCl_3$ molecules. Having checked the results with sensitive data-sources such as the far infra-red spectrum we use the computation to investigate the following dynamical properties of interacting chloroform molecules: i) transient non-Gaussian statistics; ii) the effect of non-linear restoring forces and torques in potential energy wells; iii) subtle effects of rotation/translation coupling. All three properties require a fundamental development in the analytical theory currently available.

Description of the Algorithm and Numerical Methods

The algorithm TETRA originally supplied by SERC CCP5 and written by Singer and coworkers [6] was modified to involve charge-charge interaction and a force cut-off criteria based on molecule centre of mass to centre of mass distaance (cut off radius = 12.2Å). The equations of translational motion are solved with a third-order predictor routine based on the Verlet algorithm and rotation is integrated using as coordinates the angular momentum and the three unit vectors along the principal axes [7]. The Lennard-Jones parameters are as follows: σ(H - H) = 2.75Å; σ(Cl - Cl) = 3.50Å; σ(C - C) = 3.20Å; ε/k(H - H) = 13.4K; ε/k(Cl - Cl) = 175.0K; ε/k(C - C) = 51.0K. These were taken directly from the literature and are identical with a set of Lennard-Jones parameters used in a parallel simulation [3] of CH_2Cl_2 with the one difference that σ(Cl - Cl) was adjusted to 3.50Å from 3.35Å in order to improve the pressure characteristics of the simulation. The effect of this on the angular momentum a.c.f. is illustrated in fig. (1).

In order to represent the electrostatic force field of $CHCl_3$ partial charges were taken directly from a literature calculation by del Re [8] which reproduces satisfactorily the dipole moment. This gives $q_H = 0.131|e|$; $q_H = 0.056|e|$;

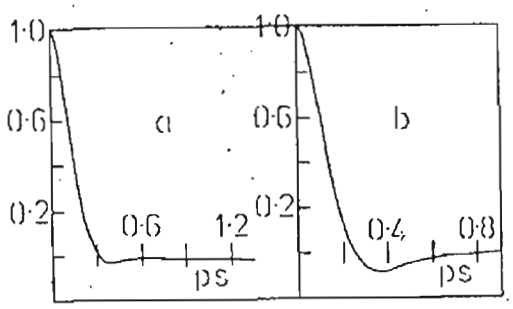

Figure (1)

Comparison of molecular dynamics simulation of the angular momentum a.c.f.'s of $CHCl_3$, at 293K, 1 bar.

a) σ = 3.35Å for the Cl - Cl interaction; b) σ = 3.50Å.

Ordinates: $\langle \underline{J}(t).\underline{J}(o)\rangle / \langle J(o).J(o)\rangle$

q_{Cl} = - 0.063|e|. Partial charge interactions are much simpler to handle than multipole-multipole interactions for a variety of reasons, not least among which is the relatively low symmetry (C_{3v}) of $CHCl_3$.

The molecules were set up intially on a solid lattice which melted over about 2000 time steps of 0.005 ps each. The main run was initiated, after rejecting these initial steps, in segments of 10 mins CPU time of the UMRCC CDC 7600 computer. Up to 10,000 more time steps were used to calculate equilibrium and time-transient properties of experimental and theoretical interest, dumping every 0.04 ps. A.C.F.'s were satisfactorily stable after about 2000 time steps but mixed a.c.f.'s required more. All correlation functions were computed with running time averages.

Equilibrium Results

The equilibrium pressure and specific heat were calculated using Cheung's equations [7]. The pressure, being a difference of two large numbers, fluctuates considerably more than any other quantity in an m.d. simulation, and is extremely sensitive to small changes in the pair potential. The specific heat at constant volume, C_V, is a fluctuation property and ideally needs runs of up to 50,000 steps for good statistics. A typical sample (after 6661 time steps) produces the following results for an inputed molar volume of liquid $CHCl_3$ corresponding to 293K, 1 bar.

$\langle T\rangle$ = 294.2K; $\langle T\rangle$(trans) = 292.9K;

$\langle T\rangle$(rot.) = 295.5K;

$\langle P\rangle$ = 24.8 ± 279 bar

$\langle$Total energy$\rangle$ = - 26.81 ± 0.07 kJmole^{-1}

$\langle$Potential energy$\rangle$ = - 34.15 kJ $mole^{-1}$

$\langle C_V \rangle$ = 42 $Jmole^{-1}K^{-1}$

These compare with experimental values [9] as follows:

$\langle$potential energy$\rangle$ = $kJmole^{-1}$

$\langle C_V \rangle$ = $Jmole^{-1}K^{-1}$

Atom-Atom Pair Distribution Functions

These measure essentially the probability of finding another atom (A) at a distance r(A) from a given atom (B) in another molecule at thermodynamic equilibrium, and are illustrated in figs. (2) to (4). X-ray and neutron diffraction measurements on liquid $CHCl_3$ are needed to corroborate these experimentally, using techniques of isotope substitution [10].

The chlorine to hydrogen p.d.f. in fig. (2) clearly shows two peaks, one very distinctly at 3.2Å might be taken as evidence for H-bonding. To corroborate this indication we must of course write algorithms to account for the effects of induction and polarisability which are molecularly non-pair-additive. The H to H atom-atom p.d.f. shows traces of four peaks, at 3.0Å, 5.2Å, 7.25Å and 9.8Å. The liquid is therefore considerably 'structured'. This is corroborated in the Cl to Cl result of fig. (3) with peaks at 3.8Å, 6.3Å and 9.0Å. There are traces of at least four peaks in the Cl to C p.d.f. of fig. (3), at 4.55Å, 5.0Å, 6.55Å (+7.0Å ?)

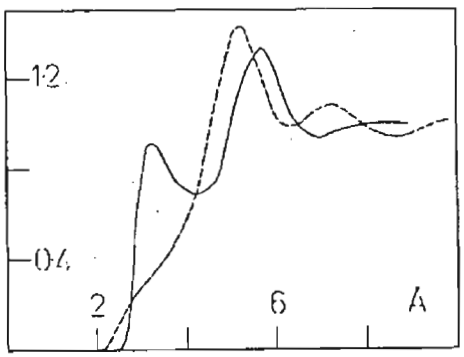

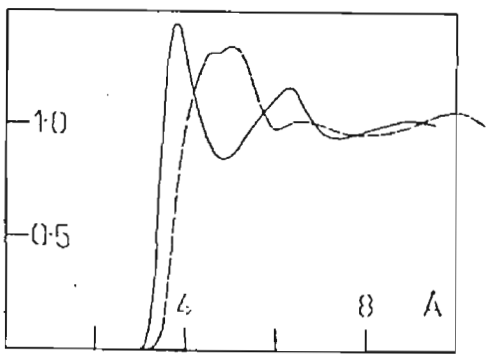

Figure (2)

Atom-atom pair distribution functions :

—— Ⓗ - Ⓒⓛ ; - - - Ⓗ - Ⓗ

Figure (3)

—— Ⓒⓛ - Ⓒⓛ ; - - - Ⓒⓛ - Ⓒ ; as for fig. (2).

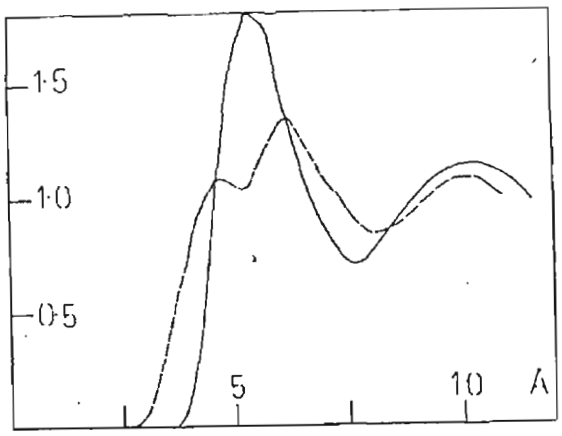

Figure (4)
—— Ⓒ - Ⓒ ; - - - Ⓒ - Ⓗ ; as for fig. (2)

and ∿10Å, although the last is uncertain because we are close to the cut off distance The C to H p.d.f. shows up three clear peaks at 4.6Å, 6.1Å and ∿10Å, and finally the C to C p.d.f. has two broad peaks around 5.4Å and probably ∿10.2Å representing nearest and next-nearest neighbouring shells. It is clear therefore that a "simple" molecular liquid such as $CHCl_3$ poses a considerable challenge to the available theories of liquid state structure". In the next section we see that the same is true for the molecular dynamics.

Time-transient Statistics

Using the fluctuation-dissipation theorem [4] these can in principle be checked against as many spectra as possible, taken from different experiments at the same state point (as in the EMLG pilot project [4,5]). The molecular dynamics algorithm deals with the following vectors: $\underline{r}_{cm}$, the centre of mass position; $\underline{v}$, the centre of mass velocity; the orientation unit vectors $\underline{e}$, $\underline{e}_2$ and $\underline{e}_3$ along the axes of the principal moment of inertia system in the molecule frame; $\underline{J}$, the angular momentum in the laboratory frame; $\underline{F}$ the force vector; $\underline{T}_q$ the torque vector; J_1, J_2 and J_3 the angular momentum components in the molecule frame; the orientational velocity vectors $\dot{\underline{e}}_1$, $\dot{\underline{e}}_2$ and $\dot{\underline{e}}_3$; the angular velocity in the laboratory frame, $\underline{\omega}$; and the position vectors of each atom in each molecule. By numerically constructing autocorrelation functions of these quantities it is possible to test directly some fundamental hypotheses of the analytical theory of, for example,

Brownian motion [12-14], and to compute experimental spectra such as that of fig.(5) in the far infra-red. The peak of the computed spectrum lies slightly below the observed peak at cm^{-1}. One of the reasons for this might be found in the fact that the simulated spectrum was built up from an autocorrelation ($\langle \dot{\underline{e}}_3(t).\dot{\underline{e}}_3(o)\rangle$) by Fourier transformation, with internal field correction; whereas the experimental spectrum is a many molecule phenomenon [15].

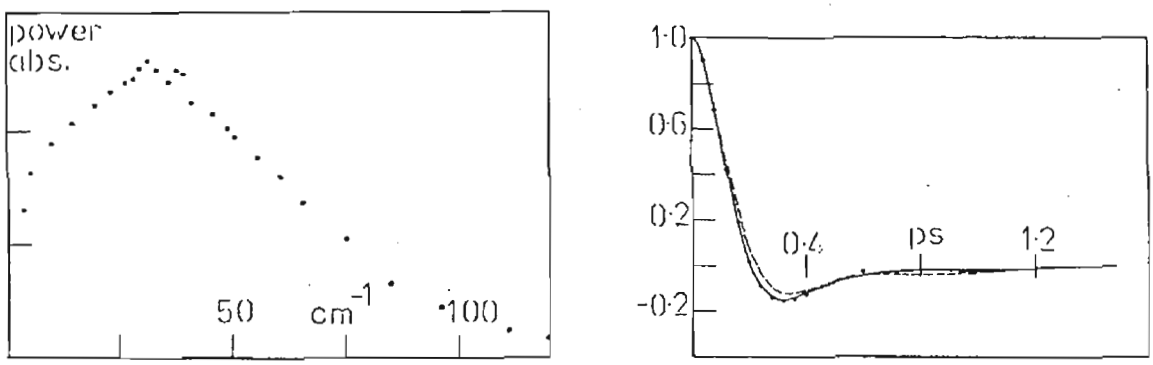

Figure (5)

Comparison of computed (0) and measured (-) far infra-red spectra for liquid $CHCl_3$ at 293K, 1 bar.

Figure (6)

Illustration of the anisotropy of rotational diffusion in $CHCl_3$

$\_\_\_\_$ $\langle \dot{\underline{e}}_3(t).\dot{\underline{e}}_3(o)\rangle / \langle \dot{\underline{e}}_3(o).\dot{\underline{e}}_3(o)\rangle$;

\- - - $\langle \dot{\underline{e}}_1(t).\dot{\underline{e}}_1(o)\rangle / \langle \dot{\underline{e}}_1(o).\dot{\underline{e}}_1(o)\rangle$

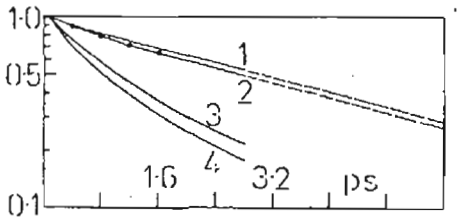

Figure (7)

Orientational a.c.f.'s for chloroform:

(1) $\langle \underline{e}_3(t).\underline{e}_3(o)\rangle$; (2) $\langle \underline{e}_1(t).\underline{e}_1(o)\rangle$;

(3) $\frac{1}{2}\langle 3(\underline{e}_3(t).\underline{e}_3(o))^2 - 1\rangle$; (4) $\frac{1}{2}\, 3(\underline{e}_1(t).\underline{e}_1(o))^2 - 1\rangle$.

By comparing the a.c.f.'s of $\dot{\underline{e}}_3$ and $\dot{\underline{e}}_1$ (fig. (6)) it is possible to see that the anisotropy of rotational diffusion in chloroform is small at 293K but definite. This is corroborated in the orientational a.c.f.'s $\langle \underline{e}_1(t).\underline{e}_1(o)\rangle$ and $\langle \underline{e}_3(t).\underline{e}_3(o)\rangle$ of fig. (7), whose correlation times are as follows. $\tau_1(\underline{e}_1) = 3.9$ ps; $\tau_2(\underline{e}_3) = 3.6$ ps; $\tau_1(\underline{e}_2) = \tau_1(\underline{e}_1)$. $\tau_2(\underline{e}_1) = \tau_2(\underline{e}_2) = 1.5$ ps; $\tau_2(\underline{e}_3) = 1.3$ ps. Here the subscripts 1 and 2 respectively denote 1st and 2nd rank in the Legendre expansion, so that $\tau_1(\underline{e}_3)$ may be linked to the dielectric relaxation time and $\tau_2(\underline{e}_3)$ and $\tau_2(\underline{e}_1)$ to the appropriate N.M.R. relaxation times or Raman relaxation times. For "rotational diffusion" $\tau_1/\tau_2 = 3.0$. The ratios for each of the vectors $\underline{e}_1$ and $\underline{e}_3$ are less than three. Interestingly the 1st rank a.c.f.'s become exponential after about 1 ps but the second rank a.c.f.'s are clearly not so up to about 2.5 ps (fig. (7)). Since these are "single particle" a.c.f.'s they are not <u>directly</u> comparable with dielectric relaxation times for chloroform. There are two ways around this problem in general. One is to compare $\tau_1(\underline{e}_3)$ with dielectric relaxation times for $CHCl_3$ in solution, and here we have 3.2 ps in cyclohexane [16], 5.0 ps in CCl_4 [16] and 4.3 ± 0.3 ps in decalin [17]. The other is to compute the "microscopic" correlation function: $\langle \underline{e}_{i3}(o).\sum_j \underline{e}_{j3}(t)\rangle$ which is shown in fig. (7). This was computed using small sub-spheres containing on average four or five molecules. The zero-time value is Kirkwood's factor for the sub-sphere. Figs. (6) and (7) both show that the a.c.f.'s and microscopic c.f.'s of $\underline{e}_3(t)$ and $\dot{\underline{e}}_3(t)$ behave similarly. The Kirkwood factor is very nearly one, which ties in with a recent analysis by Kluk and Janik [18] of freshly measured dielectric and Raman relaxation times over a wide temperature range. It is interesting therefore that $CHCl_3$ is a "<u>structured</u>" liquid (figs (2) to (4)) but dynamically isotropic as regards the molecular diffusion. Raman and N.M.R. single-particle correlation times are available from literature measurements and produce: $\tau_2(\underline{e}_3)$(N.M.R.) = $\tau_2(\underline{e}_3)$(Raman)before $p_S\tau_2(\underline{e}_1)$(N.M.R.) = $\tau_2(\underline{e}_1)$(Raman)befor ps. The difficulties of deriving times such as these experimentally are well known, involving spin-rotation analysis and vibration-rotation coupling. The broad agreement between simulation and experimentation is therefore encouraging. There are no incoherent neutron scattering measurements [10] available on liquid $CHCl_3$, but it is clear that the interpretation of such data would require a numerical simulation such as this as a guide.

Having thus established the numerical interpretation as fairly efficacious in its ability to reproduce the available experimental data we may go on to use the simulation per se as a source of new information.

Non-Gaussian Transient Statistics

The classical theory of translational Brownian motion [12] is based on the Langevin equation, which may be transformed into a Fokker-Planck equation, providing Gaussian velocity distribution of the Ornstein-Uhlenbeck process [12]:

$$G(\underline{v},t) = \left(\frac{m}{2\pi kT(1 - e^{-2\beta t})}\right)^{3/2} \exp\left[-\left(\frac{m}{2kT}\right)\frac{|\underline{v} - \underline{v}_o e^{-\beta t}|}{1 - e^{-\beta t}}\right] \quad (1)$$

Here β is the friction coefficient and $\underline{v}_o \equiv \underline{v}(o)$ the centre of mass velocity at time $t = o$. If we now define the autocorrelation functions:

$$C_1(t) = \langle \underline{v}(t).\underline{v}(o)\rangle / \langle v^2(o)\rangle \quad (2)$$

and $$C_2(t) = \langle \underline{v}(t).\underline{v}(t)\underline{v}(o).\underline{v}(o)\rangle / \langle v^4(o)\rangle \quad (3)$$

it follows [13] from eqn (1) that:

$$C_2(t) = \frac{3}{5}\left(1 + \frac{2}{3} C_1^2(t)\right) \quad (4)$$

and $$\langle v^4(o)\rangle = \frac{5}{3}\langle v^2(o)\rangle^2 \quad (5)$$

We have simulated $C_1(t)$ and $C_2(t)$ directly, and these are illustrated in fig. (8). The computer simulation accurately produces the Gaussian limit of 3/5 for $C_2(t)$ as $t \to \infty$, $C_1(t) \to o$ in eqn. (4). However eqn. (4) is not followed transiently, and the statistics for 108 molecules are not Gaussian. The same result has been reported [3,19-22] in other computer simulations, using up to 864 atoms, and therefore it seems that the analytical theory needs development.

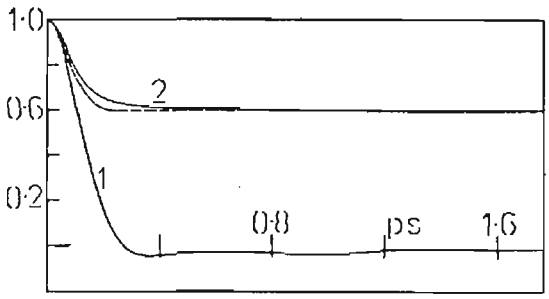

Figure (8)

Linear velocity a.c.f.'s

(1) $\langle \underline{v}(t).\underline{v}(o)\rangle / \langle \underline{v}(o).\underline{v}(o)\rangle$;

(2) $\langle \underline{v}(t).\underline{v}(t)\underline{v}(o).\underline{v}(o)\rangle / \langle v^4(o)\rangle$;

- - - Eqn. (4), the Gaussian result based on (1).

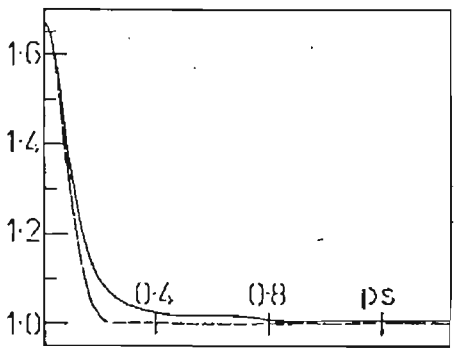

Figure (9)

Close-up of the non-Gaussian effect.

_____ $\langle \underline{v}(t).\underline{v}(t)\underline{v}(o).\underline{v}(o)\rangle / (\langle v^2(o)\rangle\langle v^2(o)\rangle)$

- - - The Gaussian result:

$$1 + \frac{2}{3}\left(\frac{\langle \underline{v}(t).\underline{v}(o)\rangle}{\langle v^2(o)\rangle}\right)^2$$

A close up of the non-Gaussian process is illustrated in fig. (9). It is clear that the difference between eqn. (4) and the computer results is intimately connected with the development of the long negative tail (fig. 8) in $C_1(t)$. This seems to suggest that the theory of isotropic Brownian motion (Ornstein/ Uhlenbeck process) should be replaced by one involving an external potential, such as considered in the Kramers equation [23]. This potential has the effect of destroying the Gaussian nature of $G(\underline{v},t)$ and of making the molecular dynamics non-linear, in the sense that the restoring force associated with the extra potential is non-linearly dependent on displacement.

The same non-linear, non-Gaussian phenomenon can be illustrated by simulating angular momentum and angular velocity a.c.f.'s in the laboratory or molecule frame. In fig. (10) we illustrate the angular momentum a.c.f. and angular velocity a.c.f. in the laboratory frame:

$$C_{J1}(t) = \langle \underline{J}(t).\underline{J}(o)\rangle / \langle J^2(o)\rangle; \tag{6}$$

$$C_{\omega_1}(t) = \langle \underline{\omega}(t).\underline{\omega}(o)\rangle \langle \omega^2(o)\rangle; \tag{7}$$

together with:

$$C_{J2}(t) = \langle \underline{J}(t).\underline{J}(t)\underline{J}(o).\underline{J}(o)\rangle / \langle J^4(o)\rangle$$

$$C_{\omega_2}(t) = \langle \underline{\omega}(t).\underline{\omega}(t)\underline{\omega}(o).\underline{\omega}(o)\rangle / \langle \omega^4(o)\rangle \tag{8}$$

To analyse the non-Gaussian nature of the angular momentum it is possible to work

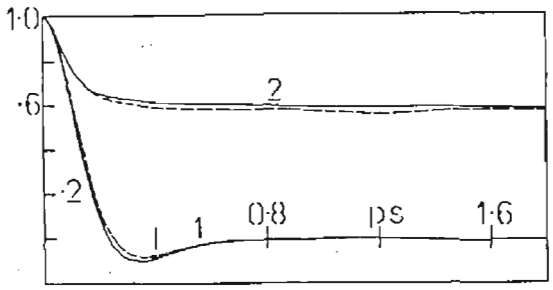

Figure (10)

(1) - - - - $\langle \underline{J}(t).\underline{J}(o)\rangle / \langle J^2(o)\rangle$

——— $\langle \underline{\omega}(t).\underline{\omega}(o)\rangle / \langle \omega^2(o)\rangle$

(2) - - - - $\langle \underline{J}(t).\underline{J}(t)\underline{J}(o).\underline{J}(o)\rangle / \langle J^4(o)\rangle$

——— $\langle \underline{\omega}(t).\underline{\omega}(t)\underline{\omega}(o).\underline{\omega}(o)\rangle / \langle \omega^4(o)\rangle$.

$\underline{J}$ = lab. frame angular momentum

$\underline{\omega}$ = " " " velocity

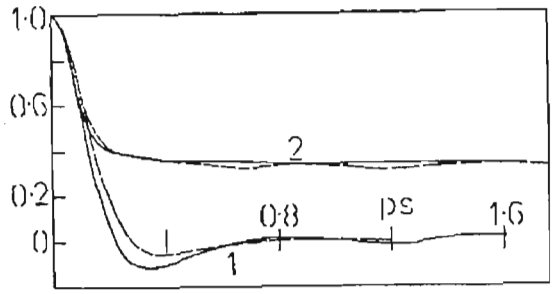

Figure (11)

Angular momentum component a.c.f.'s in the molecule fixed frame (principa- m. of I axis).

——— $\langle J_1(t)J_1(o)\rangle/\langle J_1^2(o)\rangle$

(1)

- - - $\langle J_3(t)J_3(o)\rangle/\langle J_3^2(o)\rangle$

——— $\langle J_1^2(t)J_1^2(o)\rangle/\langle J_1^4(o)\rangle$

(2)

---- $\langle J_3^2(t)J_3^2(o)\rangle/\langle J_3^4(o)\rangle$

in the molecule frame and this is illustrated in fig. (14) respectively for J_1 and J_3 a.c.f.'s as in eqns. (6) to (8). There are two sources of non-linearity (and therefore of non-Gaussianicity) in rotational molecular dynamics of this nature. The first persists in the limit of free rotation (i.e. in an infinitely dilute gas) and is due to the nature of the Euler equations. The second comes from the nature of the potential energy wells in the molecular liquid. The restoring torque here is non-linear in the angular displacement. The non-Gaussian results illustrated in fig. (11) are therefore a combination of these effects, and point towards the need for a generalised non-linear theory of molecular motion in liquids [24]. The rotational equations corresponding to eqn. (4) are given elsewhere in the literature. The first steps towards a generalised non-linear theory have been taken by Grigolini et al [25].

Rotation - Translation Effects in Chloroform

Here, the simulation is at its most incisive, because it suggests dynamic phenomena that cannot be explained in conventional terms [12]. One of these is illustrated in fig. (12) in terms of the functions $\langle J^2(o)v^2(t)\rangle/(\langle J^2(o)\times v^2(o)\rangle)$ and $\langle J^2(t)v^2(o)\rangle/(\langle J^2(o)\times v^2(o)\rangle)$. These are identical for fundamental time-

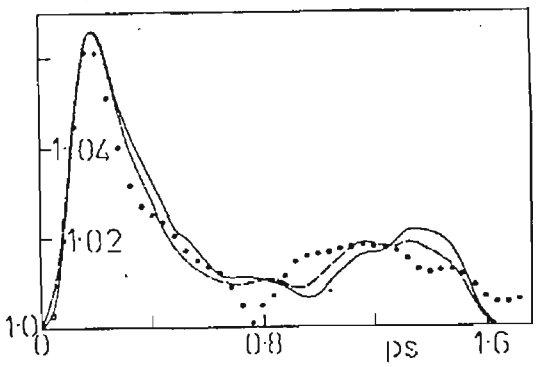

Figure (12)

—— $\langle v^2(o)J^2(t)\rangle/(\langle v^2(o)\rangle\langle J^2(o)\rangle)$

o $\langle v^2(t)J^2(o)\rangle/(\langle v^2(o)\rangle\langle J^2(o)\rangle)$

- - - As for —— with 4560 time steps as opposed to 3600 time steps total in the running time average $\langle\ \rangle$.

reversal reasons in a statistically stationary sample, and any residual difference in fig. (12) comes from the statistical noise in the simulation. Conventionally these reamin at unity for all t but the simulation shows that this is clearly not the case.

At the same time the computer simulation corroborates the theorem $\langle \underline{J}(t).\underline{v}(o)\rangle = \langle \underline{v}(t).\underline{J}(o)\rangle = o$ for all t in the laboratory frame, which comes from the symmetry of parity reversal [13]. We are therefore left with the problem of constructing a suitable joint conditional probability density function to explain the behaviour of both types of correlation function (appendix). The simulation is therefore ahead of both theory and experiment when it comes to the more subtle areas of liquid state molecular dynamics, whatever the efficacy of the potential energy function used in the equations of motion. In other words this coupling phenomenon is a fundamental new property at present detectable only by numerical means. The mixed energy a.c.f. is quite detailed in form and, as far as we can tell, has more than one peak: at 0.25 ps (well defined) and $\sim$ 1.4 ps which is very noisy. The correlation function cannot be explained by just using a Kramers equation [23], and its details are intimately connected with those of the pair potential itself. Its existence suggests a new experimentally observable phenomenon, hitherto undetected by conventional spectroscopy. A.c.f.'s such as $\dfrac{\langle \dot{e}_3^2(t)\ v^2(o)\rangle}{\langle \dot{e}_3^2(o)\rangle\langle v^2(o)\rangle}$ also exceed one for $t > o$ and are illustrated in fig. (13). Finally, in fig. (14), we show that the same type of ratio for force and torque is interestingly

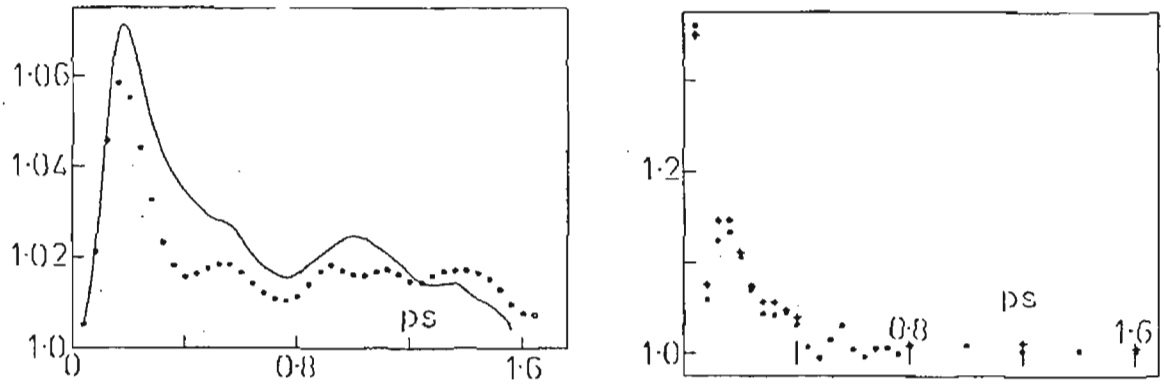

Figure (13)

——— $\langle v^2(t)\dot{e}_1^2(o)\rangle/(\langle v^2(o)\rangle\langle\dot{e}_1^2(o)\rangle)$

Θ $\langle v^2(o)\dot{e}_1^2(t)\rangle/(\langle v^2(o)\rangle\langle\dot{e}_1^2(o)\rangle)$

Figure (14)

Θ $\langle F^2(o)\underline{T}_q^2(t)\rangle/(\langle F^2(o)\rangle\langle T_q^2(o)\rangle)$

-O- $\langle F^2(t)\underline{T}_q^2(o)\rangle/(\langle F^2(o)\rangle\langle T_q^2(o)\rangle)$

$\underline{F}$ = force in the lab frame;

T_q = torque in the lab frame.

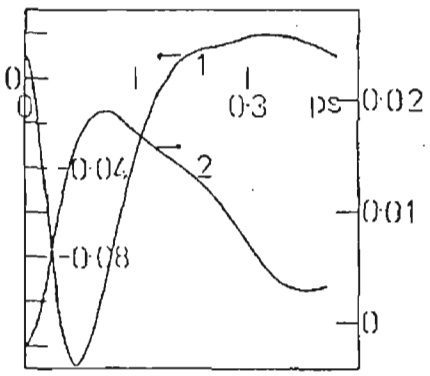

Figure (15)

The rototranslational first rank mixed a.c.f.'s $\langle\underline{v}(o)J^T(t)\rangle$ in the molecule fixed frame.

1) $\langle v_1(o)J_2(t)\rangle/(\langle v_1^2\rangle^{\frac{1}{2}}\langle J_2^2\rangle^{\frac{1}{2}})$

2) $\langle v_2(o)J_1(t)\rangle/(\langle v_2^2\rangle^{\frac{1}{2}}\langle J_1^2\rangle^{\frac{1}{2}})$

3) $\langle v_2(o)J_3(t)\rangle/(\langle v_2^2\rangle^{\frac{1}{2}}\langle J_3^2\rangle^{\frac{1}{2}})$

4) $\langle v_3(o)J_2(t)\rangle/(\langle v_3^2\rangle^{\frac{1}{2}}\langle J_2^2\rangle^{\frac{1}{2}})$

$\langle v_1(o)J_3(t)\rangle = \langle v_3(o)J_1(t)\rangle = o.$

structured around t = 0.2 ps, although in this case, of course, the initial value is > 1 because mean square force and mean square torque are not independent in the conventional statistical sense.

CONCLUSIONS

We have simulated the properties of liquid chloroform at 293K, 1bar with a model pair potential whose parameters were taken from the literature with the exception of one slight adjustment. This potential reproduces spectral properties in the far infra-red etc. fairly satisfactorily and therefore the simulation method can be used with some confidence to investigate the subtle details of $CHCl_3$ molecular dynamics and equilibrium structure.

ACKNOWLEDGEMENTS

We thank SERC CCP5 for a copy of the algorithm TETRA. The Italian CNR is acknowledged for a fellowship to MF and the Uk SERC for financial support.

APPENDIX

In this appendix we sketch out a tentative explanation of the a.c.f.'s illustrated, for example, in fig. (12).

In general the two-time, joint, conditional, transient probability distribution $P_2(X_1(t_1),\ X_2(t_2);\ \ t_2|X_1(t_1),\ X_2(t_2);\ \ t_1)$ may be written on the assumption that the overall process is Gaussian. For this we need to know the elements of the correlation matrix: $\underline{M}(t)$, $t = |t_2 - t_1|$ of the molecular dynamical variates X_1 and X_2.

$$\underline{M}(t) = \begin{bmatrix} \langle X_1(t_1)X_1(t_2)\rangle & \langle X_1(t_2)X_2(t_1)\rangle \\ \langle X_1(t_1)X_2(t_2)\rangle & \langle X_2(t_1)X_2(t_2)\rangle \end{bmatrix} \tag{A1}$$

The Gaussian distribution is:

$$P_2(\ |\ ) = \left(\frac{||(1 - \underline{M}(t)\underline{M}^T(k)||^{-1}}{(2\pi)^2}\right)$$

$$\times \exp\ -\frac{1}{2}[u(t_2) - \underline{M}(t)u(t_1)]^T$$

$$\times[\ 1 - \underline{M}(t)\underline{M}^T(t)\ ]^{-1}$$

$$\times[\ u(t_2) - \underline{M}(t)u(t_1)] \tag{A2}$$

The two time probability density for the composite process is then simply obtained by multiplying P_2 of eqn (A2) by the equilibrium joint p.d.f. P_o, which is:

$$P_o(X_1(t)\ \ X_2(t_2)\ \ t) = (2\pi\sigma_1\sigma_2(1 - R^2)^{\frac{1}{2}})^{-1}$$

$$\times \exp\ \left[\frac{1}{2(1 - R^2)}\ \left(\frac{X_1^2}{\sigma_1^2} + \frac{RX_1X_2}{\sigma_1\sigma_2} + \frac{X_2^2}{\sigma_2^2}\right)\right] \qquad \text{(A3)}$$

When dealing with $\underline{v}$ and $\underline{J}$ in the lab. frame each is a 3 - D vector with no cross-correlation [13] between their components, i.e.:

$$\langle v_i(t_1)\ J_k(t_2)\rangle_{\text{lab. frame}} = 0, \qquad \text{(A4)}$$

$$i = x, y, z;\quad k = 1, 2, 3.$$

where J_k are the three components of $\underline{J}$ along the principal moment of inertia frame.

Therefore in order to explain fig. (12) we have to use a theory based on:

$$\langle v_i(t_1)\ J_k(t_2)\rangle_{\text{mol. frame}} \neq 0 \qquad \text{(A5)}$$

Fig. (15) from the simulation clearly shows the nature of the L.H.S. in eqn. (A5). We emphasize that <u>both</u> the linear <u>and</u> angular momentum vectors have to be defined w.r.t. to the <u>molecule-fixed frame</u> for correlation to appear. Note further that

$$\langle v^2(t)\ J^2(o)\rangle_{\text{lab}} = \langle v^2(t)\ J^2(o)\rangle_{\text{molecule frame}}$$

because v^2 and J^2 are scalar quantities invariant to frame transformation.

<u>The phenomenological theory (i.e. Ornstein-Uhlenbeck theory) of molecular rototranslation must therefore be based on eqn. A5.</u>

For example, the fundamental Langevin type equation of rototranslation <u>should be</u>, for asymmetric tops:

$$\begin{aligned}\dot{\omega}_i &= (I_i - I_k)\,\omega_j\,\omega_k/I_i - \sum_{\ell=1}^{3}(\gamma_{i\ell}^{(r)}\,\omega_\ell + \gamma_{i\ell}^{(rt)}v_\ell) + T_i(t)\\ \dot{v}_i &= v_j\,\omega_k - \omega_j v_k - \sum_{\ell=1}^{3}(\gamma_{i\ell}^{(t)}v_\ell + \gamma_{i\ell}^{(tr)}\,\omega_\ell) + F_i(t)\end{aligned} \qquad \text{(A6)}$$

which is insoluble analytically. However eqn. (A6) is soluble numerically by stochastic simulation [26]. Note carefully that eqn. (A6) is written in the <u>molecule frame for both linear and</u> angular velocities $\underline{v}$ and $\underline{w}$. Ferrario [26] has solved eqn. (A6) with $\underline{v}$ in the lab frame, and the cross-correlation necessary to explain figs. (12) (13) and (15) does not exist. It remains to solve eqn. (A6) with $\underline{v}$ in the <u>molecule frame</u>, and this is work underway.

The Fokker-Planck equation equivalent to (A6) is, (in the molecule frame):

$$\frac{\partial P}{\partial t} = \sum_{i=1}^{3} -\left(\frac{\partial}{\partial_i}\left[\frac{I_i - I_k}{I_i}\right]\omega_j \omega_k P\right) + \sum_{i=1}^{3}\left(-\frac{\partial}{\partial v_i}(v_j \omega_k - v_k \omega_j) P\right)$$

$$+ \sum_{\ell=1}^{3}\left[\frac{\partial}{\partial \omega_i}\left(\gamma_{i\ell}^{(r)}\omega_\ell + \gamma_{i\ell}^{(rt)} v_\ell\right) + \frac{\partial}{\partial v_i}\left(\gamma_{i\ell}^{(t)} v_\ell + \gamma_{i\ell}^{(tr)}\omega_\ell\right)\right] P \qquad (A7)$$

$$+ \sum_{\ell=1}^{3}\left[\frac{\partial}{\partial \omega_i}\left(\gamma_{i\ell}^{(r)}\frac{kT}{I_i}\frac{\partial}{\partial \omega_\ell} + \frac{1}{2}\left(\gamma_{i\ell}^{(tr)}\frac{kT}{I_i} + \gamma_{i\ell}^{(rt)}\frac{kT}{m}\right)\frac{\partial}{\partial v_\ell}\right]\right. P$$

Eqns. (A6) or (A7) do not account for memory effects [4,5] at all, and are already difficult to solve, already impossible to solve analytically. The phenomenologocial theory of molecular rototranslation is therefore in need of development and is behind the numerical theory based on computer simulation.

Finally it is clear that rototranslation effects such as these are fundamentally important to the spectral theory of, for example, dielectrics, and in the classical theory (e.g. of Debye) are ignored. Spectral interpretation based on the theory of rotational diffusion should therefore be regarded with caution, because the theory is not only oversimplified, but fundamentally incorrect.

RE ERENCES

1 A. van der Avoird, P.E.S. Wormer, F. Mulder and R.M. Berns, "Ab Initio Studies of the Interactions in van der Waals Molecules, in "Topics in Current Chemistry", Vol. 93, ed. Dewar et al., Springer-Verlag Berlin, (1980).

2 H. Sutter, in "Dielectric and Related Molecular Processes", Vol. 1, Chem.Soc., (1972), senior rep., M. Davies.

3 M. Ferrario and M. Evans, Chem.Phys., in press.

4 M.W. Evans, G.J. Evans, W.T. Coffey and P. Grigolini, "Molecular Dynamics and Theory of Broad Band Spectroscopy", Wiley/Interscience, N.T., (1982) in press.

5 M.W. Evans, "Spectral Studies of Rotational Diffusion", Acc.Chem.Res., 14, (1981) 253.

6 K. Singer and D. Fincham, SERC CCP5 publications.

7 P.S.Y. Cheung, Mol.Phys., 33, 519 (1977); K. Singer, J.V.L. Singer and A.J. Taylor, Mol. Phys., 37, (1979) 1239.

8 R. del Re, J.Chem Soc., 36, (1958) 161.

9 "Selected Values of Chemical Thermodynamic Properties", (1961) p.588.

10 P.N. Brier and A. Perry, Adv.Mol.Int.Proc., 13, (1978) 1-46.

11 See, for example, Chem.Soc. Discussion, Canterbury, (1978).

12 N. Wax (Ed.), "Selected Papers on Noise and Stochastic Processes", Dover, N.Y., (1954).

13 B.J. Berne and R. Pecora, "Dynamic Light Scattering with Applications to Chemistry, Biology and Physics", Wiley-Interscience, N.Y., (1976).

14 J.H. Calderwood and W.T. Coffey, Proc. R.Soc. London, 356A,

15 C. Brot, ref. (2), vol. 2, p.1.

16 N.B.S. circular No. 501.

17 C.J. Reid, Ph.D. Thesis, Univ. of Wales (1979).

18 E. Kluk and B. Janik, to be published.

19 A. Rahman, Phys.Rev., 136, (1964) 405.

20 B.J. Berne and G.D. Harp, Adv.Chem.Phys., 17, (1970) 63.

21 G.J. Evans, M.W. Evans and W.T. Coffey, Adv.Mol.Rel.Int.Proc., 20,(1981) 11.

22 U. Balucani, V. Tognetti, R. Vallauri, P. Grigolini and M.P. Lombardo, Phys. Letters, submitted.

23 M. Ferrario, M. Evans and W.T. Coffey, Adv.Mol.Rel.Int.Proc., 20 (1981) p.1.

24 M. Ferrario, P. Marin, P. Grigolini and M.W. Evans, in preparation.

25 P. Grigolini and P. Marin, paper presented at EUCIOS 15, EMLG session, J.Mol. Structure, in press; P. Grigolini, M. Ferrario and M.W. Evans, Physica A, in press; P. Grigolini, M. Giordano and P. Marin, Chem.Phys. Letters, in press; P. Grigolini and M. Ferrario, Chem.Phys. Letters, 62, (1979) 100.

26 M. Ferrario, to be published.